THE JOURNAL OF BIOLOGICAL CHEMISTRY VOL. 288, NO. 5, pp. 3419–3427, February 1, 2013

Unique Features of the Anti-parallel, Heterodimeric Coiled-coil Interaction between Methyl-cytosine Binding Domain 2 (MBD2) Homologues and GATA Zinc Finger Domain Containing 2A (GATAD2A/p66α)*

Received for publication, October 26, 2012, and in revised form, December 7, 2012 Published, JBC Papers in Press, December 13, 2012, DOI 10.1074/jbc.M112.431346

Ninad M. Walavalkar[‡§], **Nathaniel Gordon**[¶], **and David C. Williams, Jr.**[§1]

From the [‡]*Integrative Life Sciences Program,* [§]*Department of Pathology and the Massey Cancer Center, Virginia Commonwealth University, Richmond, Virginia 23298 and* [¶]*Eastern Virginia Medical School, Norfolk, Virginia 23501*

Background: The MBD2-p66α coiled-coil interaction is key to the function of the NuRD chromatin remodeling complex.
Results: Binding to p66α depends on helicity and electrostatic potential of the MBD2 domain.
Conclusion: Variations in helical content and charge distribution dictate a binding affinity hierarchy for MBD2 homologues.
Significance: Delineating determinants of binding will aid the development of inhibitors of these complexes.

The methyl-cytosine binding domain 2 (MBD2)-nucleosome remodeling and deacetylase (NuRD) complex recognizes methylated DNA and silences expression of associated genes through histone deacetylase and nucleosome remodeling functions. Our previous structural work demonstrated that a coiled-coil interaction between MBD2 and GATA zinc finger domain containing 2A (GATAD2A/p66α) proteins recruits the chromodomain helicase DNA-binding protein (CHD4/Mi2β) to the NuRD complex and is necessary for MBD2-mediated DNA methylation-dependent gene silencing *in vivo* (Gnanapragasam, M. N., Scarsdale, J. N., Amaya, M. L., Webb, H. D., Desai, M. A., Walavalkar, N. M., Wang, S. Z., Zu Zhu, S., Ginder, G. D., and Williams, D. C., Jr. (2011) p66α-MBD2 coiled-coil interaction and recruitment of Mi-2 are critical for globin gene silencing by the MBD2-NuRD complex. *Proc. Natl. Acad. Sci. U.S.A.* 108, 7487–7492). The p66α-MBD2 interaction differs from most coiled-coils studied to date by forming an anti-parallel heterodimeric complex between two peptides that are largely monomeric in isolation. To further characterize unique features of this complex that drive heterodimeric specificity and high affinity binding, we carried out biophysical analyses of MBD2 and the related homologues MBD3, MBD3-like protein 1 (MBD3L1), and MBD3-like protein 2 (MBD3L2) as well as specific mutations that modify charge-charge interactions and helical propensity of the coiled-coil domains. Analytical ultracentrifugation analyses show that the individual peptides remain monomeric in isolation even at 300 μM in concentration for MBD2. Circular dichroism analyses demonstrate a direct correlation between helical content of the coiled-coil domains in isolation and binding affinity for p66α. Furthermore, complementary electrostatic surface potentials and inherent helical content of each peptide are necessary to maintain high-affinity association. These factors lead to a binding affinity hierarchy of p66α for the different MBD2 homologues (MBD2 ≈ MBD3 > MBD3L1 ≈ MBD3L2) and suggest a hierarchical regulatory model in tissue and life cycle stage-specific silencing by NuRD complexes.

The coiled-coil domain represents a relatively simple yet common protein-protein interaction motif found in as many as 10% of all eukaryotic proteins (2). Recent work has shown that selective disruption of coiled-coil complexes can target specific protein complexes for potential therapeutic benefit (1, 3). Coiled-coils form specific homo- or hetero-oligomeric complexes involving 2–7 α-helices in parallel or anti-parallel arrangements important for a wide variety of cellular functions either on their own or as a part of larger protein complexes (2, 4–6). Most studies to date have described the formation of parallel homo-oligomeric coiled-coils, whereas the anti-parallel heterodimeric coiled-coil complexes are relatively understudied (3, 4). Here we investigate the biophysical properties of the antiparallel heterodimeric coiled-coil interaction between MBD2 homologues and p66α[2] critical for methyl-cytosine binding domain 2 (MBD2)-mediated, DNA methylation-dependent gene silencing.

At least five MBD proteins have been identified in humans that share a homologous MBD that selectively binds methylated DNA: MeCP2 and MBD1 through MBD4. Each of these proteins contains a unique sequence outside of the MBD and recruits distinct co-regulatory complexes to silence expression of the associated gene, with the notable exception of MBD2 and MBD3 which share >65% identity (7–11). MBD2 and MBD3 proteins recruit the NuRD chromatin remodeling complex comprised by histone deacetylase (HDAC1/2), p66α/β, metastasis associated (MTA1/2/3), retinoblastoma binding

* This work was supported, in whole or in part, by National Institutes of Health Grant R01-GM098264 (to D. C. W.). This work was also supported by American Cancer Society ACS IRG-73–001 (to D. C. W.).

[1] To whom correspondence should be addressed: Dept. of Pathology, Virginia Commonwealth University, P. O. Box 980035, Richmond, VA 23298-0035. Tel.: 804-628-2073; Fax: 804-828-2812; E-mail: dwilliams8@mcvh-vcu.edu.

[2] The abbreviations used are: p66α, GATA zinc finger containing domain 2A; MBD2 and -3, methyl-cytosine binding domain proteins 2 and 3; MBD3L1 and -L2, methyl-cytosine binding domain 3-like proteins 1 and 2; NuRD, nucleosome remodeling and deacetylase complex; ITC, isothermal titration calorimetry; AUC, analytical ultracentrifugation; APBS, Adaptive Poisson-Boltzmann Solver.

(RbAp46/48), and chromodomain helicase DNA binding (CHD4/Mi2β) proteins (12–14). We recently demonstrated that the highly conserved and homologous C-terminal coiled-coil regions of MBD2 and MBD3 form a high affinity heterodimeric complex with p66α critical for recruitment of the Mi2 protein and methylation dependent gene silencing *in vivo* (1). MBD3-like protein 1 (MBD3L1) and MBD3-like protein 2 (MBD3L2) are MBD2 homologues that lack the methyl-CpG-binding domain but contain a coiled-coil domain (Fig. 1*A*) and can recruit an intact NuRD complex. MBD3L2 is expressed in germ cell tumors and some somatic tissues, whereas MBD3L1 is testis-specific and expressed in post-meiotic spermatids (15, 16). In Fig. 1*B* the key residues that are involved in making hydrophobic and polar/ionic interactions with the coiled-coil of p66α are highlighted. Given the similarities and differences between these homologous domains, we have pursued detailed analysis of the different homologous to gain a better understanding of the structural determents for high affinity binding.

A coiled-coil domain can be identified by a regular seven amino acid (**a**-**g**) repeat of hydrophobic and charged residues (5, 6). In this heptad repeat, a branched hydrophobic residue is present at **a** and **d** positions, whereas charged/polar residues are present at **e** and **g**. These seven residues form approximately two turns of a typical α-helix, generating a hydrophobic face (**a** and **d**) bordered by charged/polar residues (**e** and **g)**. Two or more of these α-helices bind along this hydrophobic interface and, because the natural rotation of this surface, the helices tend to wrap around one another forming a "coil of coils." This arrangement is capable of forming either parallel or anti-parallel hetero- or homo-oligomeric complexes ranging from 2 to 7 helices. Despite this seemingly simple paradigm, subtle variations in sequence can have dramatic consequences on binding specificity, stoichiometry, and parallel *versus* anti-parallel alignment (17).

In the studies presented here we show that high affinity binding requires preformed helical content as well as specific charged residues on the individual coiled-coil domains. The reduction in helical content of the isolated MBD3L1 and MBD3L2 homologues reduces binding affinity for p66α. We previously demonstrated that changing the charge of three residues in p66α eliminates binding to wild type MBD2 (1). Introducing complementary charge changes in MBD2 restores binding but not with the same high affinity as wild type. Based on electrostatic potential calculations, we suggest that the uniquely high affinity association of the wild type complex depends on complementary alternating positive and negative electrostatic potential surfaces. Hence variations in both the helical content and electrostatic interactions between MBD2 homologues lead to a relative binding affinity hierarchy for p66α (MBD2 $\approx$ MBD3 $>$ MBD3L1 $\approx$ MBD3L2).

EXPERIMENTAL PROCEDURES

Protein Preparation—The coiled-coil regions of human MBD2b (amino acids 211–244), MBD3 (amino acids 216–249), MBD3L1 (amino acids 145–178), MBD3L2 (amino acids 166–199), and p66α (amino acids 138–178) were cloned and expressed with a hexahistidine tag and as thioredoxin fusion proteins in a modified pET32a vector (18). The expression vectors were transformed into the BL21(DE3) *Escherichia coli* strain, grown in Luria Bertani medium at 37 °C, and induced with 1 mM isopropyl-β-D-thiogalactopyranoside at an $A_{600} \sim 0.8$. The bacteria were harvested after 2 h of induction and lysed with the B-PER reagent (Thermo Scientific). The soluble fraction was passed over a nickel-Sepharose column, and protein was eluted with a step gradient of imidazole and further purified by gel filtration over a Superdex-75 column (GE Healthcare). The thioredoxin fusion proteins were used directly for analytical ultracentrifugation (AUC) and isothermal titration calorimetry (ITC) studies. For circular dichroism (CD) studies, clones were modified to incorporate a tyrosine residue just after the thrombin cleavage site (for quantification of the isolated peptide by UV) and were expressed in a similar manner. After purification over a nickel-Sepharose column, the peptides were cleaved by thrombin digest and isolated by gel filtration chromatography over a Superdex-75 column (GE Healthcare). Specific mutations were introduced using the QuikChange® site-directed mutagenesis kit (Stratagene) following the manufacturers protocol. The final concentrations of all protein samples were determined by UV absorbance at 280 nm.

Analytical Ultracentrifugation—Sedimentation velocity experiments were carried out using Beckman Optima XL-I analytical ultracentrifuge (Beckman Coulter Inc.) equipped with a four and eight-position AN-60Ti rotor. Sedimentation was performed at 40,000 rpm, 20 °C, under physiological buffer conditions (20 mM Tris, pH 8.0, 150 mM NaCl). Sedimentation profiles were recorded using UV absorption (280 nm) and interference scanning optics. The partial specific volume ($\bar{V}$) of the sample, density (ρ), and viscosity (η) of the buffer were calculated using the SEDNTERP program (19). Data were fit using a continuous size distribution ($c(s)$), and the effective molecular weight was determined from the resulting sedimentation coefficients with the SEDFIT software (20).

Isothermal Titration Calorimetry—Protein samples were prepared in standard buffer (Tris, pH 8.0, 150 mM NaCl), and binding was analyzed with an iTC_{200} Microcalorimeter (GE Healthcare). A total of 24 injections (1.5 μl each) of the p66α coiled-coil (100 μM) were injected into MBD2 and homologues (10 μM, 298 K, stir speed of 400 rpm, 120 s time delay between injections). The resulting isotherms were auto-adjusted for base line and fit to a one-site binding model using Origin 7.0 software to determine binding constant ($K_D K_a^{-1}$) and enthalpy (ΔH), whereas the Gibbs free energy (ΔG) and entropy (ΔS) of binding were calculated according to Equation 1,

$$RT\ln(K) = \Delta G - \Delta H - T\Delta S \qquad \text{(Eq. 1)}$$

where T is the temperature in Kelvin, and R is the gas constant.

Circular Dichroism—CD spectra were collected on purified peptide samples (~33 μg/ml total protein in 10 mM sodium phosphate, pH 6.5) with a JASCO J-715 CD spectrometer (JASCO Corp) at 293 K with a 1-cm path length scanning from 190 to 260 nm with 0.5-nm interval at a scanning speed of 50 nm/min. CD spectra were normalized to give molar ellipticity values (θ) in degrees·cm^{-2}·dmol^{-1}residue^{-1}. Helical content for each peptide was calculated from the ratio of the observed $\theta_{222\,nm}$ to the expected $\theta_{222\,nm}$ for 100% helix as given by

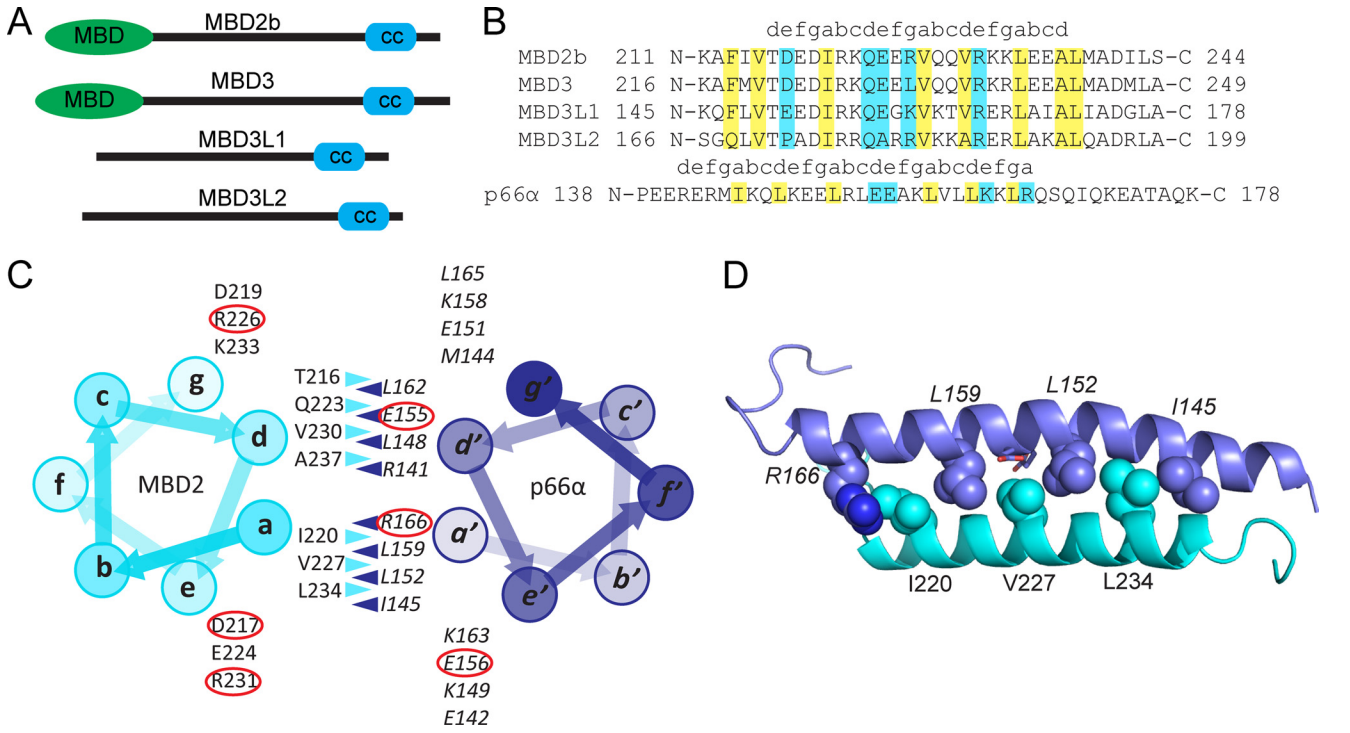

FIGURE 1. **The coiled-coil interaction between MBD2 homologues and p66α.** The domain organization (*A*) is diagramed for MBD2 and homologues, which shows that the MBD3L1 and MBD3L2 proteins lack a methyl-cytosine binding domain. A sequence alignment (*B*) of the coiled-coil (*cc*) domains from p66α and MBD2 homologues is shown with key hydrophobic (*yellow*) and ionic/polar (*cyan*) contact residues highlighted and the heptad repeat (**a-g**) indicated *above the amino acid sequences*. A helical wheel diagram of the complex (*C*) highlights the interacting residues at positions **a**, **d**, **g**, and **e** of the heptad repeat with key charged residues circled in *red*. A ribbon diagram of the p66α-MBD2 coiled-coil complex (*D*) is shown with the branched hydrophobic residues at the **a** position on each chain depicted as *spheres* and the two central glutamates (*E155* and *E156*) of p66α depicted as *sticks*.

40,000 × ((n − 4)/n), where n is the number of residues (21). Thermal denaturation was followed at $\theta_{222\ nm}$ from 277 to 368 K at 1 K intervals with a heating rate of 1 K/min. The data were fit to a simple two state thermodynamic model of unfolding as described by Koepf *et al.* (22).

Helical Content Prediction—The expected helical content for each peptide was calculated using the AGADIR (23, 24) algorithm with the N and C termini "free" at 293 K, ionic strength of 0.02, and pH 6.5 to closely match the experimental conditions for CD. The predicted helical content was used to help design amino acid changes that stabilize helix formation.

Electrostatic Surface Potential—The coordinates of the isolated wild type coiled-coil domains were extracted from the previously determined solution structure (PDB code 2L2L), and the surface potential was calculated with the Adaptive Poisson-Boltzmann Solver (APBS) (25). The coiled-coil domains of the different mutants and homologous domains were derived from the wild type MBD2 structure by introducing appropriate sequence differences with the mutagenesis function of PyMOL (26) and choosing a side-chain rotamer that did not sterically collide with neighboring residues. The calculated electrostatic potential was mapped to the solvent-accessible surface with the APBS plugin tool in PyMOL (26) and colored from red to blue (−1 to +1 eV, respectively).

RESULTS

Conservation of Hydrophobic Interactions—The key contact residues in the MBD2 coiled-coil domain are conserved across all homologues, with MBD3L2 composed of the most divergent sequence (44% identity between MBD2 and MBD3L2 coiled-coil domains), whereas MBD3 and MBD2 are nearly identical (93% identity). Anti-parallel coiled-coils form sequential intermolecular interactions between branched hydrophobic residues at **a** and **a′** as well as **d** and **d′** positions of the heptad repeat in the two chains. Recent work indicates that select triplet repeats at the **a′-a-a′** positions favor heterodimeric coiled-coil formation, with LIL or ILI triplets the most favored combination (27). As can be seen in Fig. 1, the **a** positions are identical across all MBD2 homologues with the **a-a′** interactions composed by *RILVLLI* (p66α residues are in italics throughout). This arrangement includes two favorable I-L pairings and one of the more favorable triplets, LVL. The highly conserved valine residue of this triplet inserts into a pocket between two conserved glutamate residues at a central bend in the p66α helix (Fig. 1*D*). The shorter valine side chain (as compared with isoleucine and leucine residues) allows close approximation of the two helices, which likely contributes to close intermolecular ionic interactions involving the glutamate residues. The conserved **d-d′** interactions (28), which are composed of *LQEV*(A)*LA*, also place a valine (or alanine in MBD3L2) at the bend on the p66α helix near these same glutamate residues.

The Coiled-coils of MBD2, MBD3, MBD3L1, and MBD3L2 Are Largely Monomeric in Isolation—Although coiled-coil domains often form homo-oligomeric interactions, we previously demonstrated that both MBD2 and p66α remain monomeric in isolation (1). To test for homo-oligomerizaton of the different homologues as well as the concentration dependence

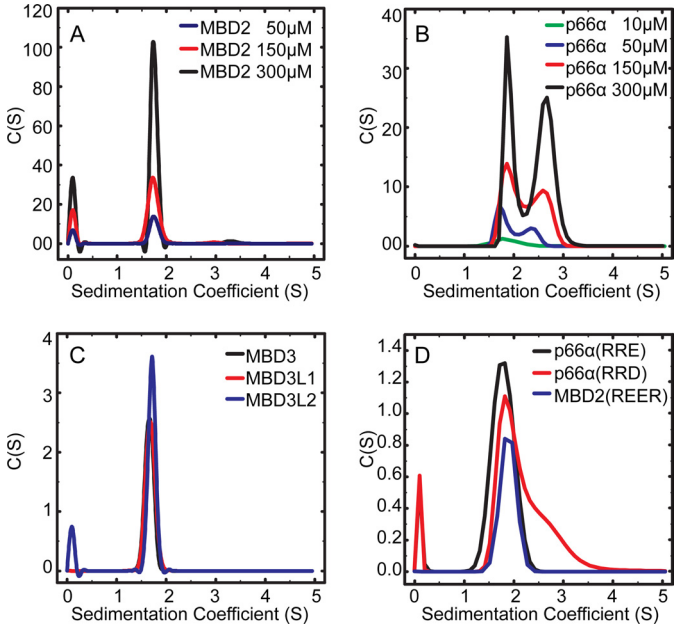

FIGURE 2. **The coiled-coil domains remain largely monomeric in isolation.** Analytical ultracentrifugation analysis was performed on the individual coil domains and the sedimentation velocity fit using a continuous size distribution ($c(s)$). The results are shown for increasing concentrations of MBD2 (*A*) and p66α (*B*) coiled-coil domains as well as for 50 μM concentrations of the coiled-coil domains from MBD3, MBD3L1, and MBD3L2 (*C*) and MBD2 and p66α mutants (*D*).

of homodimerization of MBD2 and p66α, we carried out sedimentation velocity AUC studies. The MBD2 coiled-coil domain remains monomeric even at concentrations up to 300 μM (Fig. 2*A*). On the other hand, the p66α coiled-coil shows a tendency to form a homodimer at concentration beyond 50 μM (Fig. 2*B*); however, the monomer remains the dominant species up to 300 μM. Given the low nanomolar binding constant between MBD2 and p66α coiled-coil domains, p66α preferentially forms a stable heterodimer with MBD2 rather than a homodimer. Similarly, AUC analyses showed that the coiled-coil domains of MBD3, MBD3L1, and MBD3L2 homologues remain stable monomers at 50 μM concentrations (Fig. 2*C*).

Binding Analysis of MBD2 Homologues Reveals a Hierarchical Affinity Preference for the p66α Coiled-coil—ITC was performed using thioredoxin fusion constructs of the coiled-coil domains. Exothermic heat was generated with each injection in all experiments. The binding isotherms are shown in Fig. 3*A*, and the measured binding affinity (K_D), free energy (ΔG), enthalpy (ΔH), and entropy ($-T\Delta S$) for each homologue is provided in Table 1. These results show that p66α binds with higher affinity to MBD3 ($K_D = 23 \pm 3$ nM) and MBD2 (K_D 42 $\pm$ 9 nM) as compared with MBD3L1 ($K_D = 377 \pm 34$ nM) and MBD3L2 ($K_D = 268 \pm 32$ nM). Each complex binds with a stoichiometry of ~1:1 (n ranges from 0.7 to 1.4, Table 1) consistent with heterodimer formation. The reduced binding affinity of p66α for the MBD3L1 and MBD3L2 homologues reflects a more unfavorable change in entropy upon binding ($-T\Delta S =$ 0.17 and 6.3 kcal/mol for MBD2 and MBD3L1, respectively) that is not fully compensated by a more favorable change in enthalpy ($\Delta H = -10.2$ and -15.1 kcal/mol for MBD2 and MBD3L1, respectively).

Although the coiled-coil domains do not contain a histidine residue or other titratable protons at a pH of 8.0, the high ionization enthalpy of Tris buffer (11.4 kcal/mol) (29) could contribute to the apparent enthalpy change upon binding. To address this possibility, we repeated ITC for MBD2-p66α in PIPES buffer (20 mM PIPES, pH 7.5, 150 mM NaCl), which has a much lower ionization enthalpy (2.7 kcal/mol) (29). The binding constant and change in enthalpy are very similar in PIPES ($K_D = 30 \pm 11$ nM, $\Delta H = -10.8 \pm 0.2$ kcal/mol, $-T\Delta S = 0.56$ kcal/mol), which indicates that complex formation does not involve net transfer of a proton.

High Affinity Binding Depends on the Helical Content of the Isolated Coiled-coil Domains—We previously demonstrated that the MBD2 and p66α coiled-coil domains show a strong tendency to form monomeric helices in isolation (1). An algorithm based on helix-coil transition theory (AGADIR (23, 24)) predicts that the MBD3L1 and MBD3L2 homologues do not have the same tendency to form α-helices in isolation (Table 2). CD analyses were performed on the isolated domains, which confirmed the relative helical content of the homologous coiled-coil domains in isolation. MBD2 (25%) and MBD3 (28%) are more helical than MBD3L1 (7%) and MBD3L2 (11%) (Fig. 4*A*). The thermal stability of the different coiled-coil complexes was determined by following molar ellipticity at 222 nm ($\theta_{222\ nm}$) as a function of temperature. Complexes involving MBD2 and MBD3 melt at a higher temperature than those involving MBD3L1 and MBD3L2, consistent with the higher binding affinities of MBD2 and MBD3.

To test whether helical content dictates high affinity association, we introduced mutations at residues opposite the binding interface of the coiled-coil domains of MBD2 and MBD3L1 that reduce or increase helical content, respectively. A glycine for glutamate substitution in the middle of the helix opposite the binding interface could contribute to the reduced helical content of MBD3L1 (Fig. 1*B*). Consistent with *in silico* calculations, the G159E mutation of MBD3L1 increases helical content (7% to 16%, Table 2), whereas the E225G mutation of MBD2 reduces helical content (25% to 9%, Table 2). As expected, the binding affinity for the p66α coiled-coil domain (Table 1) and the melting temperature of the complex increased for MBD3L1 G159E ($K_D = 44$ nM, $T_m = 331$ K), which is close to the affinity of wild-type MBD2 ($K_D = 42$ nM, $T_m = 338$ K) and much greater than wild-type MBD3L1 ($K_D = 377$ nM, $T_m = 319$ K). In contrast, the binding affinity and melting temperature of MBD2 E225G ($K_D > 50$ μM, $T_m = 313$ K) was greatly decreased as compared with wild type. Because this residue is on the side of the helix opposite the binding surface and does not directly interact with p66α, these findings support the hypothesis that high affinity association requires pre-existing helical content.

Specific Ionic Interactions Are Required for High Affinity Coiled-coil Complex Formation—We recently demonstrated that mutating specific charged residues of p66α reduces binding affinity by 3 orders of magnitude when introduced separately (either *E155R/E156R* or *R166E*) and abolishes complex formation when introduced together (*E155R/E156R/R166E*) (1). These residues form close ionic interactions with three charged residues in MBD2 (Asp-217, Arg-226, and Arg-231) that are conserved across all MBD2 homologues (Fig. 1*B*)

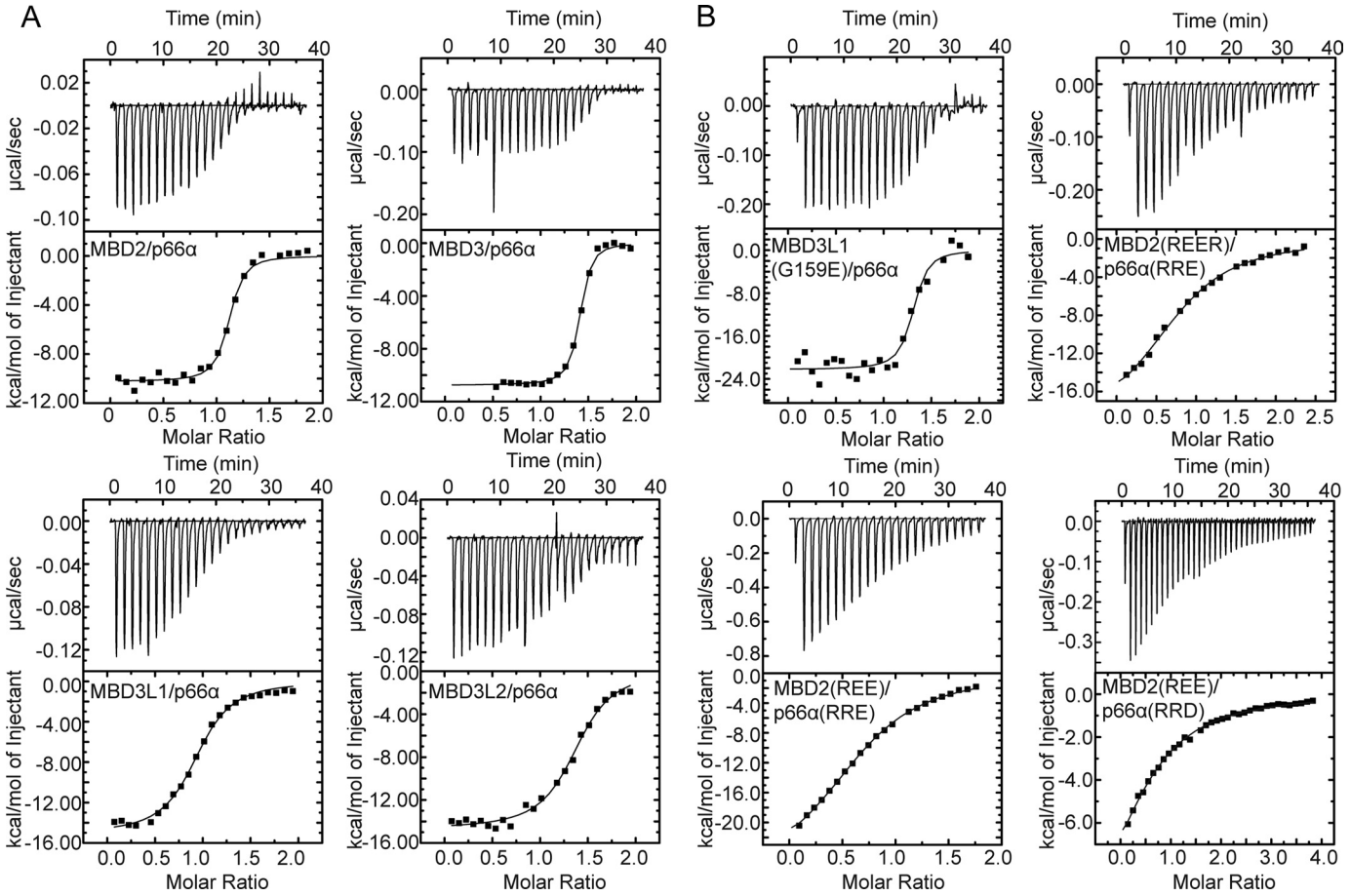

FIGURE 3. **Binding analysis of MBD2 homologues and mutants.** Isothermal titration calorimetry studies were performed, and the experimental data (*top panel*) and resulting fit (*bottom panel*) are shown for MBD2, MBD3, MBD3L1, and MBD3L2 coiled-coil domains binding to the p66α coiled-coil domain (*A*) and for the coiled-coil domains of MBD3L1(G159E) binding to p66α, MBD2(REE), and MBD2(REER) binding to p66α(RRE) and MBD2(REE) binding to p66α(RRD) (*B*).

TABLE 1

Binding affinity analyses

The dissociation constant (K_D), change in enthalpy (ΔH), entropy ($-T\Delta S$), Gibbs free energy (ΔG), and apparent stoichiometry (n) derived from isothermal titration calorimetry studies are given for wild type and mutant coiled-coil complexes between p66α and MBD2 homologues. In addition, the melting temperatures (T_m) derived from circular dichroism studies are given for complexes that show high affinity.

Coiled-coil complex	*n*	*K*	Δ*H*	−*T*Δ*S*	Δ*G*	T_m
		nM	*kcal/mol*	*kcal/mol*	*kcal/mol*	*K*
MBD2/p66α	1.1	42 ± 9	−10.2 ± 0.1	0.17	−10.0 ± 0.1	338
MBD3/p66α	1.4	23 ± 3	−10.8 ± 0.1	0.35	−10.4 ± 0.1	332
MBD3L1/p66α	0.9	377 ± 34	−15.1 ± 0.2	6.3	−8.8 ± 0.1	319
MBD3L2/p66α	1.4	268 ± 32	−14.7 ± 0.2	5.7	−9.0 ± 0.2	308
MBD2(REE)/p66α(RRE)	0.7	10,800 ± 400	−27.1 ± 0.4	20.3	−6.8 ± 0.4	
MBD2(REE)/p66α(RRD)	1.2	38,000 ± 2000	−13.9 ± 1.1	7.9	−6.0 ± 1.1	
MBD2(REER)/p66α(RRE)	0.8	5,400 ± 500	−20.0 ± 0.7	12.8	−7.2 ± 0.7	
MBD2(REER)/p66α(RRD)	0.7	33,000 ± 9800	−16.3 ± 1.1	10.2	−6.1 ± 1.1	
MBD2(E225G)/p66α		≥ 50,000				
MBD3L1(G159E)/p66α	1.3	44 ± 20	−22.2 ± 0.5	12.2	−10.0 ± 0.5	331

and likely provide specificity for the coiled-coil interaction. Based on this observation, we hypothesized that introducing complementary changes in MBD2 would restore high affinity binding.

Introducing the D217R/R226E/R231E mutations in MBD2 (MBD2(REE)) does restore binding to the and p66α *E155R/E156R/R166E* mutant (p66α(RRE)). However, ITC analysis (Fig. 3*B*) indicates a much lower affinity between the mutant proteins (K_D = 10.8 μM) than wild type. *In silico* calculations with AGADIR as well as CD measurements show that mutating these residues decreased the α-helical content of MBD2 (9% *versus* 25%, Table 2). These changes introduced an unfavorable charge interaction between Glu-231 and Glu-235 residues of MBD2(REE). To increase helicity, a fourth mutation (E235R) was introduced to increase the helical content (as predicted by AGADIR) without disrupting intermolecular contacts. The D217R/R226E/R231E/E235R mutant MBD2 (MBD2(REER)) did show an increase in helical content (36% *versus* 9%, Table 2), and ITC revealed a slight increase in binding affinity (5.4 μM) for p66α(RRE) as compared with MBD2(REE) but still approximately 2 orders of magnitude lower than for the wild type complex.

TABLE 2

Helical content of the isolated coiled-coil domains

The percent helix as predicted by AGADIR and calculated from the circular dichroism molar ellipticity at 222 nm ($\theta_{222\,nm}$) is given for the wild type and mutant coiled-coil domains.

Coiled-coil domain	Helical propensity in isolation	
	Predicted[a]	Calculated[b]
	%	
MBD2	40	25
MBD3	48	28
MBD3L1	11	7
MBD3L2	8	11
MBD2(E225G)	11	9
MBD3L1(G159E)	25	16
MBD2(REE)	7	9
MBD2(REER)	21	36
p66α	55	66
p66α(ERR)	56	60

[a] Based on the AGADIR algorithm.
[b] Based on circular dichroism measurements.

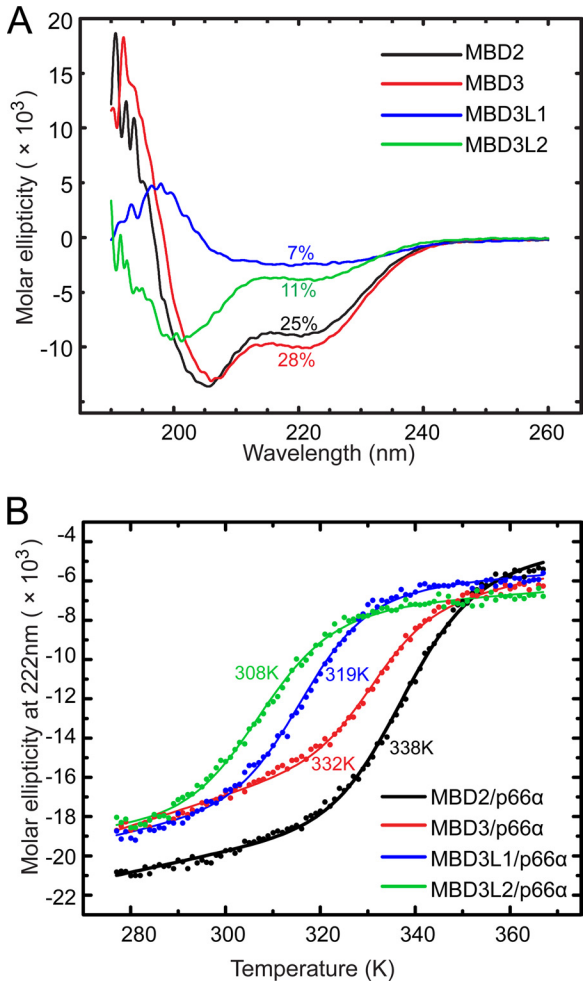

FIGURE 4. **The helical content and thermal denaturation of MBD2 homologues.** Circular dichroism spectra (*A*) of the coiled-coil domains from MBD2 homologues in isolation are shown and labeled with the helical content as calculated from $\theta_{222\,nm}$. The temperature dependence of $\theta_{222\,nm}$ (*B*) is shown from 277 to 368 K for coiled-coil complexes between the MBD2 homologues and p66α. The data were fit to a simple two-state unfolding model (22), and the resulting thermal denaturation curves labeled with the melting temperature (T_m).

One potential difference between the wild type and mutant complexes is that the favorable Arg-166-Asp-217 p66α-MBD2 ionic interaction was replaced by Glu-166-Arg-217 in the mutant complex. The additional carbon atom in glutamate (as compared with aspartate) could alter the geometry and prohibit favorable interaction. However, both MBD2(REE) and MBD2(REER) bound to p66α(RR**D**) with lower affinity than p66α(RRE) (Table 1), demonstrating that this difference was not responsible for the lower binding affinity.

Alternatively, swapping glutamate and arginine residues between chains could alter the geometric relationship between the charged residues by changing the relative positions of the two residues on the helical backbone. Changes in the relative positions of these residues could preclude ideal interaction and prevent high affinity association. Geometrical restraints are particularly important for hydrogen bond formation. Hence, to probe this possibility we tested whether geometrically restrained bidentate hydrogen bonds could be formed between the p66α-MBD2 intermolecular ionic pairs of Arg-166-Asp-217 or Glu-156-Arg-231 and the respective charge swap mutations. We introduced hydrogen bond distance and angle restraints and performed simulating annealing calculations (XPLOR_NIH (30)) while keeping the coordinates fixed for all backbone atoms and the side-chain atoms for all amino acids exclusive of the four under consideration. As can be seen in Fig. 5*A*, reasonable hydrogen-bond distances and angles can be established between these side chains in both the wild type and mutant complexes, suggesting that geometric constraints do not prevent optimal interaction in either case.

The MBD2 and p66α Coiled-coil Domains Have Highly Complementary Electrostatic Surface Potentials—To investigate differences between the wild type and charge swap complexes, the electrostatic potential of the individual peptides were calculated by the APBS (25) and mapped to the surface with the APBS plugin tool in PyMOL (26). This analysis reveals that the wild type peptides have complementary alternating positive (*blue*) and negative (*red*) surface potentials (Fig. 5*B*). The MBD3, MBD3L1, and MBD3L2 homologues show a very similar pattern (Fig. 5*D*). The **a** and **a′** hydrophobic "knobs" are largely positioned where the surface potentials change from positive to negative (indicated by *arrows* in Fig. 5*B*).

The electrostatic surface potential of the charge swap mutations are highly complementary as well (Fig. 5*C*), indicating that the chosen mutations did restore the specific charge interactions. However, the interaction surfaces on each of the mutant peptides are more uniformly positive (p66α) or negative (MBD2). Hence the hydrophobic knobs are now positioned within a more uniform electrostatic charge potential.

DISCUSSION

Here we have presented biophysical analyses of the heterodimeric anti-parallel coiled-coil complex between p66α and MBD2 homologues. This represents one of the few studies of a native anti-parallel coiled-coil complex and, to our knowledge, the only such study comparing a family of homologous coiled-coil domains. The p66α-MBD2 complex demonstrates several unusual features including the propensity of the individual domains to form monomeric helices in isolation, a clear lack of oligomerization for MBD2 even at fairly high concentrations (300 μM), and a requirement for minimum helical content in isolation to bind with high affinity.

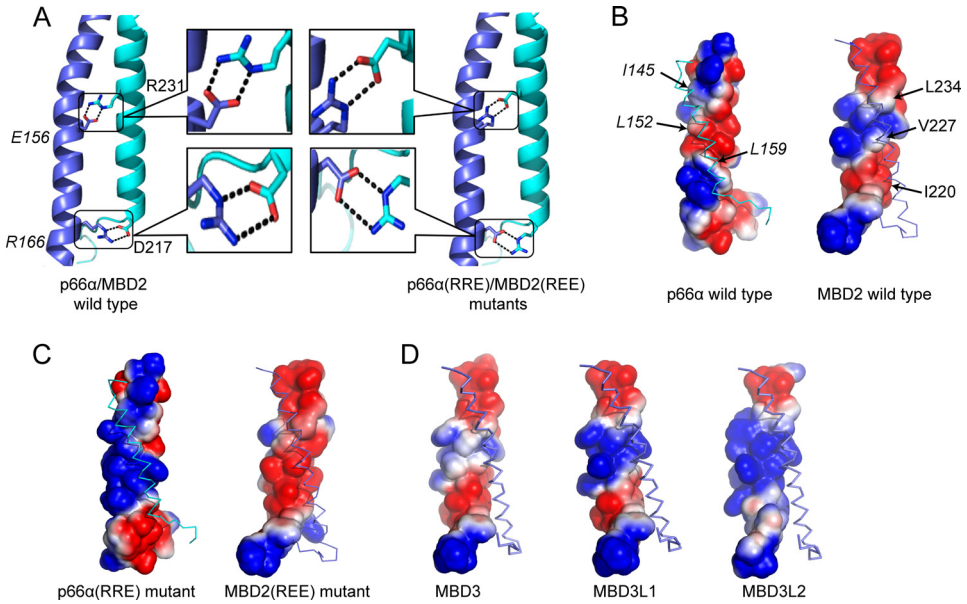

FIGURE 5. **Ionic interactions and electrostatic surface potentials of the coiled-coil complex.** To test whether geometric constraints prevent close interaction between charged residues in the charge swap mutant proteins, bidentate hydrogen bond restraints between p66α-MBD2 residues Arg-166-Asp-217 and Glu-156-Arg-231 (and the respective charge swap mutations) were incorporated, and the side-chain conformations were minimized by simulated annealing molecular dynamic calculations. Representative minimized structures (*A*) are shown for both the wild type and mutant complexes; the minimized charged side chains are depicted as *sticks*, and the bidentate hydrogen bonds are indicated by *dashed lines*. The electrostatic surface potentials for wild type (*B*) and mutant (*C*) p66α and MBD2 coiled-coil domains as well as for MBD3, MBD3L1, and MBD3L2 coiled-coil domains (*D*) were calculated with the APBS (25) tool in PyMOL (26) and the surface potential colored from *red* to *blue* (−1 to +1 eV). The intermolecular contact surface is shown for each with the binding partners depicted as a ribbon diagram for orientation. The location of hydrophobic residues at **a** and **a′** positions are indicated with *arrows* (*B*) for the wild type peptides.

Comparing the different homologous coiled-coil domains, we find that the MBD2 and MBD3 domains bind with an ~10-fold greater affinity than either the MBD3L1 or MBD3L2 domains. This difference reflects a larger unfavorable change in entropy that is not fully compensated by a more favorable change in enthalpy change when comparing MBD3L1 and MBD3L2 with MBD2. These changes correlate with the observation that MBD3L1 contains less preformed helical content than MBD2 (7% *versus* 25%, respectively). Hence MBD3L1 binding to p66α involves a coil to helix transition that reduces internal degrees of freedom yielding a large unfavorable change in entropy while at the same time forming backbone hydrogen bonds of an α helix providing a favorable enthalpy change. Furthermore, mutating a non-contact glutamate of MBD2 to a glycine (E225G) reduces helical content (from 25% to 9%) and greatly reduces the binding affinity, whereas the reverse mutation in MBD3L1 (G159E) increases helical content (from 7% to 16%) and increases binding affinity. Taken together, these experiments show that high affinity binding requires minimal preformed helical content of the individual coiled-coil domains.

This requirement for preformed helical content differs from other coiled-coil complexes that often show evidence of a coil to helix transition upon binding (31). For example, binding and folding of the GCN4 coiled-coil dimerization domain has been well characterized with conflicting results. In general, thermodynamic unfolding of GCN4 reflects a two-state transition such that binding appears coupled to folding (32). However, NMR (33) and mutation analyses (34) indicate that pre-existing helical content promotes complex formation. In contrast to earlier studies (35), the latter results suggest that the transition state involves interaction between preformed helical segments (36). In more recent studies of the oligomerization domain (SARAH) from serine/threonine mammalian sterile 20-like kinase (MST1), thermodynamic analyses show that this coiled-coil domain remains unstructured in isolation and folds upon binding (31). The unstructured state of the monomeric SARAH domain allows the protein to adopt different structures and bind different partners. In contrast to these prior studies, the coiled-coil domains of MBD2 and homologues do not form homodimeric complexes. The lack of homodimerization simplified analysis and allowed us to probe the relationship between helical content of the MBD2 monomer with heterodimer formation.

Given the propensity to form helices in isolation and the large hydrophobic surface of the coiled-coil domains, one would anticipate that the individual peptides should homo-oligomerize in isolation, especially at high concentration. However AUC analyses show that the coiled-coil domains of MBD2 and each of the homologues do not homo-oligomerize. In fact, the MBD2 remains entirely monomeric even at 300 μM concentration (Fig. 2*A*). Therefore, the coiled-coil domains do not form homo- or heterodimeric complexes between the different homologues as has been suggested previously. Instead these domains remain isolated monomeric helices until binding p66α as a 1:1 complex.

As we demonstrated previously (1), charged residues contributed to binding specificity such that reversing the charge of three residues in p66α eliminates binding to MBD2. Here we have shown that introducing complementary charge changes in MBD2 restores binding to the charge mutant of p66α but not with the same high affinity as the wild type complex. The inabil-

ity to bind with high affinity does not reflect a lack of helical content nor does it reflect geometric restraints on the relative positioning of the charged residues. Therefore, we hypothesize that the electrostatic surface potential generated by these charged residues contributes to high affinity association. The wild type electrostatic surface potential alternates between positive and negative regions such that the branched hydrophobic residues (at position **a**) fall at the interface between these oppositely charged regions. In contrast, the surface potentials for the mutant proteins are more uniformly positive (p66α(ERR)) or negative (MBD2(REE)). Even though the charge swap mutations generate complementary electrostatic surface potentials, these surface potentials are qualitatively different from the wild type proteins. Based on these observations we suggest that optimal high affinity binding between MBD2 and p66α depends on the alternating surface potential. One possibility for this requirement is that the position of the hydrophobic residues between alternating surface potentials may stabilize induced dipole moments and increase van der Waals interactions between the two chains.

These studies underscore how small changes in helical content and electrostatic interactions can modulate the binding affinity of the coiled-coil domains. In this case, the changes led to a 10-fold binding affinity preference of p66α for MBD2 and MBD3 over the MBD3L1 and MBD3L2 homologues. MBD3L1 and MBD3L2 homologues are expressed in specific tissue types (15), whereas MBD2 and MBD3 are more ubiquitous. Each of these proteins recruits the same NuRD chromatin remodeling complex; however, MBD3L1 and MBD3L2 lack a methyl-cytosine binding domain (Fig. 1*A*) and as such target the complex to distinct regions (15, 16, 37).

In previous studies we showed that the coiled-coil interaction between p66α and MBD2 was critical for the formation of a functional NuRD complex (1). Enforced expression of the isolated p66α peptide blocked recruitment of the native p66α protein and the Mi2 chromatin remodeling protein. Consequently the p66α peptide blocked DNA methylation-dependent gene silencing by the MBD2 protein. The relative binding hierarchy of the MBD3 homologues indicates that the ubiquitously expressed MBD2 and MBD3 should effectively compete with MBD3L1 and MBD3L2 for a functional NuRD in those cell types that co-express the homologous proteins. In this manner, fine-tuning of coiled-coil domain binding affinity can be used to establish hierarchical binding networks for tissue-specific gene regulation and chromatin remodeling.

In summary, we have shown that differences in helical content and charge distribution dictate high affinity anti-parallel heterodimeric coiled-coil complex formation between MBD2 homologues and p66α. The MBD2 homologues remain monomeric helices in isolation, even at high concentrations, poised to bind p66α with high affinity and specificity. Although the coiled-coil domain represents a relatively simple binding motif, subtle variations in sequence can modify binding affinity and specificity. Understanding the determinants of high affinity binding will inform the development of inhibitors of coiled-coil complexes for potential therapeutic benefit (3).

Acknowledgments—We thank Ellis Bell for help with CD studies and Carlos R. Escalante, Rahul Jaiswal, and Francisco Zarate-Perez for help with ITC and AUC analyses.

REFERENCES

1. Gnanapragasam, M. N., Scarsdale, J. N., Amaya, M. L., Webb, H. D., Desai, M. A., Walavalkar, N. M., Wang, S. Z., Zu Zhu, S., Ginder, G. D., and Williams, D. C., Jr. (2011) p66α-MBD2 coiled-coil interaction and recruitment of Mi-2 are critical for globin gene silencing by the MBD2-NuRD complex. *Proc. Natl. Acad. Sci. U.S.A.* **108,** 7487–7492
2. Grigoryan, G., and Keating, A. E. (2008) Structural specificity in coiled-coil interactions. *Curr. Opin. Struct. Biol.* **18,** 477–483
3. Strauss, H. M., and Keller, S. (2008) Pharmacological interference with protein-protein interactions mediated by coiled-coil motifs. *Handb. Exp. Pharmacol.* **186,** 461–482
4. Testa, O. D., Moutevelis, E., and Woolfson, D. N. (2009) CC+. A relational database of coiled-coil structures. *Nucleic Acids Res.* **37,** D315–D322
5. Steinmetz, M. O., Jelesarov, I., Matousek, W. M., Honnappa, S., Jahnke, W., Missimer, J. H., Frank, S., Alexandrescu, A. T., and Kammerer, R. A. (2007) Molecular basis of coiled-coil formation. *Proc. Natl. Acad. Sci. U.S.A.* **104,** 7062–7067
6. Burkhard, P., Stetefeld, J., and Strelkov, S. V. (2001) Coiled coils. A highly versatile protein folding motif. *Trends Cell Biol.* **11,** 82–88
7. Zhang, Y., Ng, H. H., Erdjument-Bromage, H., Tempst, P., Bird, A., and Reinberg, D. (1999) Analysis of the NuRD subunits reveals a histone deacetylase core complex and a connection with DNA methylation. *Genes Dev.* **13,** 1924–1935
8. Hendrich, B., and Tweedie, S. (2003) The methyl-CpG binding domain and the evolving role of DNA methylation in animals. *Trends Genet.* **19,** 269–277
9. Hendrich, B., Guy, J., Ramsahoye, B., Wilson, V. A., and Bird, A. (2001) Closely related proteins MBD2 and MBD3 play distinctive but interacting roles in mouse development. *Genes Dev.* **15,** 710–723
10. Hendrich, B., and Bird, A. (1998) Identification and characterization of a family of mammalian methyl-CpG binding proteins. *Mol. Cell. Biol.* **18,** 6538–6547
11. Fatemi, M., and Wade, P. A. (2006) MBD family proteins. Reading the epigenetic code. *J. Cell Sci.* **119,** 3033–3037
12. Bowen, N. J., Fujita, N., Kajita, M., and Wade, P. A. (2004) Mi-2/NuRD. Multiple complexes for many purposes. *Biochim. Biophys. Acta* **1677,** 52–57
13. Denslow, S. A., and Wade, P. A. (2007) The human Mi-2/NuRD complex and gene regulation. *Oncogene* **26,** 5433–5438
14. Wade, P. A. (2001) Methyl CpG-binding proteins and transcriptional repression. *Bioessays* **23,** 1131–1137
15. Jiang, C. L., Jin, S. G., Lee, D. H., Lan, Z. J., Xu, X., O'Connor, T. R., Szabó, P. E., Mann, J. R., Cooney, A. J., and Pfeifer, G. P. (2002) MBD3L1 and MBD3L2, two new proteins homologous to the methyl-CpG-binding proteins MBD2 and MBD3. Characterization of MBD3L1 as a testis-specific transcriptional repressor. *Genomics* **80,** 621–629
16. Jin, S. G., Jiang, C. L., Rauch, T., Li, H., and Pfeifer, G. P. (2005) MBD3L2 interacts with MBD3 and components of the NuRD complex and can oppose MBD2-MeCP1-mediated methylation silencing. *J. Biol. Chem.* **280,** 12700–12709
17. Yadav, M. K., Leman, L. J., Price, D. J., Brooks, C. L., 3rd, Stout, C. D., and Ghadiri, M. R. (2006) Coiled coils at the edge of configurational heterogeneity. Structural analyses of parallel and antiparallel homotetrameric coiled coils reveal configurational sensitivity to a single solvent-exposed amino acid substitution. *Biochemistry* **45,** 4463–4473
18. Cai, M., Williams, D. C., Jr., Wang, G., Lee, B. R., Peterkofsky, A., and Clore, G. M. (2003) Solution structure of the phosphoryl transfer complex between the signal-transducing protein IIA^{Glucose} and the cytoplasmic domain of the glucose transporter IICB^{Glucose} of the *Escherichia coli* glucose phosphotransferase system. *J. Biol. Chem.* **278,** 25191–25206
19. Lebowitz, J., Lewis, M. S., and Schuck, P. (2002) Modern analytical ultracentrifugation in protein science. A tutorial review. *Protein Sci.* **11,**

2067–2079
20. Schuck, P. (2000) Size-distribution analysis of macromolecules by sedimentation velocity ultracentrifugation and lamm equation modeling. *Biophys. J.* **78,** 1606–1619
21. Kumita, J. R., Smart, O. S., and Woolley, G. A. (2000) Photo-control of helix content in a short peptide. *Proc. Natl. Acad. Sci. U.S.A.* **97,** 3803–3808
22. Koepf, E. K., Petrassi, H. M., Sudol, M., and Kelly, J. W. (1999) WW. An isolated three-stranded antiparallel β-sheet domain that unfolds and refolds reversibly; evidence for a structured hydrophobic cluster in urea and GdnHCl and a disordered thermal unfolded state. *Protein Sci.* **8,** 841–853
23. Muñoz, V., and Serrano, L. (1994) Elucidating the folding problem of helical peptides using empirical parameters. *Nat. Struct. Biol.* **1,** 399–409
24. Lacroix, E., Viguera, A. R., and Serrano, L. (1998) Elucidating the folding problem of α-helices. Local motifs, long-range electrostatics, ionic-strength dependence, and prediction of NMR parameters. *J. Mol. Biol.* **284,** 173–191
25. Baker, N. A., Sept, D., Joseph, S., Holst, M. J., and McCammon, J. A. (2001) Electrostatics of nanosystems. Application to microtubules and the ribosome. *Proc. Natl. Acad. Sci. U.S.A.* **98,** 10037–10041
26. Schrödinger, L. (2010) The PyMOL Molecular Graphics System, Version~1.3r1, Schrodinger, LLC, New York
27. Hadley, E. B., Testa, O. D., Woolfson, D. N., and Gellman, S. H. (2008) Preferred side-chain constellations at antiparallel coiled-coil interfaces. *Proc. Natl. Acad. Sci. U.S.A.* **105,** 530–535
28. Steinkruger, J. D., Bartlett, G. J., Hadley, E. B., Fay, L., Woolfson, D. N., and Gellman, S. H. (2012) The d′–d–d′ vertical triad is less discriminating than the a′–a–a′ vertical triad in the antiparallel coiled-coil dimer motif. *J. Am. Chem. Soc.* **134,** 2626–2633
29. Doyle, M. L. (2001) Titration microcalorimetry. *Curr. Protocols Protein Sci.* 20.4.1–20.4.24
30. Schwieters, C. D., Kuszewski, J. J., Tjandra, N., and Clore, G. M. (2003) The Xplor-NIH NMR molecular structure determination package. *J. Magn. Reson.* **160,** 65–73
31. Constantinescu Aruxandei, D., Makbul, C., Koturenkiene, A., Lüdemann, M. B., and Herrmann, C. (2011) Dimerization-induced folding of MST1 SARAH and the influence of the intrinsically unstructured inhibitory domain. Low thermodynamic stability of monomer. *Biochemistry* **50,** 10990–11000
32. Dragan, A. I., and Privalov, P. L. (2002) Unfolding of a leucine zipper is not a simple two-state transition. *J. Mol. Biol.* **321,** 891–908
33. Myers, J. K., and Oas, T. G. (1999) Reinterpretation of GCN4-p1 folding kinetics. Partial helix formation precedes dimerization in coiled coil folding. *J. Mol. Biol.* **289,** 205–209
34. Zitzewitz, J. A., Ibarra-Molero, B., Fishel, D. R., Terry, K. L., and Matthews, C. R. (2000) Preformed secondary structure drives the association reaction of GCN4-p1, a model coiled-coil system. *J. Mol. Biol.* **296,** 1105–1116
35. Sosnick, T. R., Jackson, S., Wilk, R. R., Englander, S. W., and DeGrado, W. F. (1996) The role of helix formation in the folding of a fully α-helical coiled coil. *Proteins* **24,** 427–432
36. Moran, L. B., Schneider, J. P., Kentsis, A., Reddy, G. A., and Sosnick, T. R. (1999) Transition state heterogeneity in GCN4 coiled coil folding studied by using multisite mutations and crosslinking. *Proc. Natl. Acad. Sci. U.S.A.* **96,** 10699–10704
37. Jiang, C. L., Jin, S. G., and Pfeifer, G. P. (2004) MBD3L1 is a transcriptional repressor that interacts with methyl-CpG-binding protein 2 (MBD2) and components of the NuRD complex. *J. Biol. Chem.* **279,** 52456–52464